

# Structural and Computational Assessment of the Influence of Wet-Chemical Post-Processing of the Al-Substituted Cubic $\text{Li}_7\text{La}_3\text{Zr}_2\text{O}_{12}$

Robert Kun,<sup>\*,†,‡,§,||</sup> Frederieke Langer,<sup>‡</sup> Massimo Delle Piane,<sup>||</sup> Saneyuki Ohno,<sup>⊥,||</sup> Wolfgang G. Zeier,<sup>⊥,||</sup> Michael Gockeln,<sup>†</sup> Lucio Colombi Ciacchi,<sup>§,||</sup> Matthias Busse,<sup>‡,§</sup> and István Fekete<sup>#</sup>

<sup>†</sup>Faculty of Production Engineering, Innovative Sensor- and Functional Materials Research Group, University of Bremen, Badgasteiner Str. 1, 28359 Bremen, Germany

<sup>‡</sup>Fraunhofer Institute for Manufacturing Technology and Advanced Materials - IFAM, Wiener Str. 12, 28359 Bremen, Germany

<sup>§</sup>MAPEX Center for Materials and Processes, University of Bremen, Bibliothekstr. 1, 28359 Bremen, Germany

<sup>||</sup>Faculty of Production Engineering and Bremen Center for Computational Materials Science, University of Bremen, Am Fallturm 1, 28359 Bremen, Germany

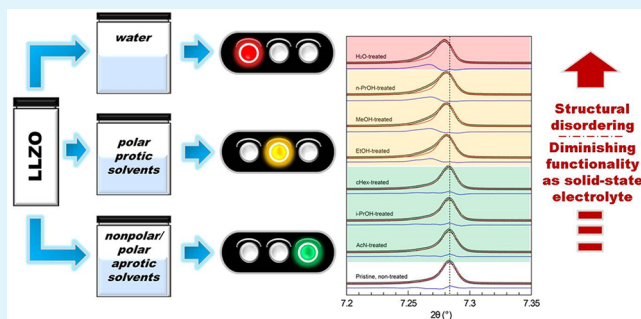
<sup>⊥</sup>Institute of Physical Chemistry, Justus-Liebig-University Giessen, Heinrich-Buff-Ring 17, 35392 Giessen, Germany

<sup>#</sup>Department of Physical Geography and Informatics, Soil- and Water Analysing Laboratory, University of Szeged, Egyetem u. 2, 6722 Szeged, Hungary

## Supporting Information

**ABSTRACT:**  $\text{Li}_7\text{La}_3\text{Zr}_2\text{O}_{12}$  (LLZO) and related compounds are considered as promising candidates for future all-solid-state Li-ion battery applications. Still, the processing of those materials into thin membranes with the right stoichiometry and crystal structure is difficult and laborious. The sensitivity of the Li-ion conductive garnets against moisture and the associated  $\text{Li}^+/\text{H}^+$  cation exchange makes their processing even more difficult. Formulation of suitable polymer/ceramic hybrid solid state electrolytes could be a prosperous way to reach the future large scale production of solid state Li-ion batteries. In fact, solvent mediated and/or slurry based wet-processing of the LLZO, e.g., tape-casting, could result in irreversible Li-ion loss of the pristine material due to  $\text{Li}^+/\text{H}^+$  cation exchange. The concomitant structural changes and loss in functionality in terms of Li-ion conductivity are the results of the above process. Therefore, in the present work a systematic study on the chemical stability and structural retention of Al-substituted LLZO in different solvents is reported. It was found that  $\text{Li}^+/\text{H}^+$  exchange in LLZO occurs upon solvent immersion, and its magnitude is dependent on the availability of  $-\text{OH}$  functional groups of the solvent molecules. As a result, a larger degree of  $\text{Li}^+/\text{H}^+$  exchange causes higher increase of the lattice parameter of the LLZO, determined by synchrotron diffraction analyses. The expansion of the cubic unit cell was ascertained, when  $\text{Li}^+$  was replaced by  $\text{H}^+$  in the host lattice, by ab initio computational studies. The application of the most common solvent as dispersion medium, i.e., high purity water, causes the most significant  $\text{Li}^+/\text{H}^+$  exchange and, therefore, structural change, while acetonitrile was proven to be the best suitable solvent for wet postprocessing of LLZO. Finally, computational calculations suggested that the  $\text{Li}^+/\text{H}^+$  exchange could result in diminished ionic, i.e., mixed  $\text{Li}^+-\text{H}^+$ , conductivity due to the insertion of protons with lower mobility than that of Li-ions.

**KEYWORDS:** garnet type  $\text{Li}_7\text{La}_3\text{Zr}_2\text{O}_{12}$ , lithium ion conductor, solvent compatibility, wet-processing, composite electrolyte, all-solid-state Li-ion battery



## INTRODUCTION

With the rising demand for portable electronic devices and electromobility, energy storage systems with increased energy density and significantly enhanced safety are needed. All-solid-state lithium ion batteries are considered as an improvement of commercially available lithium ion batteries based on liquid electrolytes regarding both safety and energy density.<sup>1</sup> By replacing the flammable, organic liquid electrolyte with a

nonflammable solid alternative, the safety of the battery cell could be increased. Furthermore, using solid state electrolytes is thought to enable the use of lithium metal as the negative electrode material along with high voltage positive electrode

**Received:** June 13, 2018

**Accepted:** October 8, 2018

**Published:** October 8, 2018

materials, thereby increasing the energy density of the battery cell. Recently, several materials have been considered as suitable solid state electrolytes. Among them, the garnet type oxide ceramics with the approximate formula of  $\text{Li}_7\text{La}_3\text{Zr}_2\text{O}_{12}$  (LLZO) have been found to be promising materials. The cubic crystal modification with acceptable high ionic conductivity is usually stabilized using various substitution elements, such as aluminum,<sup>2,3</sup> gallium,<sup>4</sup> or tantalum.<sup>5</sup>

Recently, the combination of ceramic garnets with polymer electrolytes has attracted attention to form “hybrid” or composite electrolytes. Several attempts have been made to create composites of LLZO and polymer electrolytes to realize thin membranes. In the most facile way, LLZO particles are dispersed in a solution consisting of the polymer electrolyte precursors, namely, the polymer (usually poly(ethylene oxide) (PEO)) and a lithium salt (lithium perchlorate ( $\text{LiClO}_4$ ) or lithium bis(trifluoromethanesulfonyl)imide ( $\text{LiTFSI}$ )) dissolved in an organic solvent (e.g., acetonitrile).<sup>6–11</sup> The dispersion is cast onto a flat surface and dried. Other processing techniques for garnets are tape casting a solution and drying/sintering the ceramic slurry, hot-pressing the polymer–ceramic mixture,<sup>12</sup> or infiltrating an electrospun ceramic scaffold with a polymer electrolyte solution.<sup>13–15</sup> In all cases, solvents are needed to process the ceramic. By using wet postprocessing steps such as tape casting, slurry based blade-coating for the fabrication of LLZO powders into Li-ion conductive polymer/ceramic membranes, the applied solvents have to match several requirements. Being chemically inert against LLZO and a good solvent for both Li-salt and applied polymer is especially important. Polar protic solvents such as water or alcohol homologues are good solvents for many Li-salts and polymers such as PEO. However, the intimate contact and the treatment of the LLZO with water may result in leaching out the mobile  $\text{Li}^+$ -ion species from the oxide ceramic.

It has been shown that LLZO garnets are sensitive to humidity,<sup>16,17</sup> reacting to form  $\text{LiOH}$  in the first step, followed by the reaction with atmospheric  $\text{CO}_2$  to form  $\text{Li}_2\text{CO}_3$  eventually.<sup>17–21</sup> The underlying mechanism behind this reaction is a lithium/proton ( $\text{Li}^+/\text{H}^+$ ) cation exchange process. Very recently, the significant deterioration of the Li-ion transfer kinetics in partially protonated  $\text{Li}_{6.55}\text{Ga}_{0.15}\text{La}_3\text{Zr}_2\text{O}_{12}$  by water treatment was experimentally demonstrated.<sup>22</sup> However, the advantageous effect of the  $\text{Li}^+/\text{H}^+$  cation exchange during highly dense full-ceramic membrane processing have been also demonstrated recently.<sup>23,24</sup> As it can be conceived, protonation (i.e.,  $\text{Li}^+/\text{H}^+$  cation exchange) of the cubic LLZO could positively affect its densification during the combined casting–sintering membrane process by introducing additional densification reaction mechanisms between the formed  $\text{Li}_2\text{CO}_3$  and the constituent oxides of the LLZO.

The stability of the Li-ion conducting garnet structures has been investigated regarding the structure stability of proton exchanged garnet forms.<sup>25,26</sup> In these experiments, LLZO was stirred in water for several days<sup>27</sup> or acidic media<sup>25</sup> to achieve high ion exchange rates. Further attempts of proton exchange have been made by treating pristine powders with ethanol/benzoic acid solution.<sup>25,26</sup> In all cases, changes in the crystal structure were observed. For small proton exchange rates, an increase in the lattice parameters was observed, while for high proton exchanges rates (small Li content remaining in the garnet) a change from a symmetric to a non-centro-symmetric space group was detected.<sup>25,27</sup> The aim of the previous investigations was to identify changes in crystal structure as a

function of the proton content in the lattice and the location of the protons in the garnet structure. A comprehensive review of proton exchange of Li garnet materials in aqueous media was recently published by Thangadurai et al.<sup>28</sup> Nevertheless, the results raise questions about garnet stability in other liquid media used during wet postprocessing steps at ambient temperatures without further heat treatment of the solvent-treated LLZO garnets.

In that sense, solvent compatibility of Li-ion conductive garnets is of great importance with respect to materials science and especially the processing/manufacturing technology. In the present study we report a systematic study of structural changes of Al-substituted  $\text{Li}_7\text{La}_3\text{Zr}_2\text{O}_{12}$  (LLZO) on solvent treatments. The magnitude of the  $\text{Li}^+/\text{H}^+$  exchange upon solvent treatment of the pristine powder was probed by optical emission spectroscopy (ICP-OES). Structural changes in the Al-substituted LLZO by  $\text{Li}^+/\text{H}^+$  cation exchange were investigated by synchrotron X-ray diffraction analyses combined with ab initio computational studies.

The magnitude of  $\text{Li}^+/\text{H}^+$  exchange and the resulting variations in the lattice parameter ( $a$ ) of the cubic LLZO were determined dependent on solvent chemistry. On immersion of LLZO into solvents with different chemistries, the  $\text{Li}^+/\text{H}^+$  cation exchange occurred to different degrees. This in turn resulted in structural changes in the solvent treated Al-substituted LLZO powders. The observed  $\text{Li}^+/\text{H}^+$  cation exchange might ultimately deteriorate Li-ion conductivity of the solid-state Li-ion electrolyte. Accordingly, an assessment of the most suitable solvents as dispersion media for LLZO using the wet-chemical postprocessing route is reported.

## EXPERIMENTAL SECTION

**1. Sample Preparation.** LLZO powder was prepared by a coprecipitation technique and described elsewhere.<sup>3</sup> Briefly, constituent metal nitrates were dissolved in aqueous solution and precipitated as hydroxides using an ammonium hydroxide solution. To stabilize the cubic structure, 0.25 per formula unit  $\text{Al}^{3+}$  was added as a substitution element. The precipitate was dried afterward and mixed with lithium salt. To account for lithium losses during calcination, excess lithium (10 mol %) was used. The dried hydroxide precipitate/lithium salt mixture was calcined at 850 °C to yield high purity, cubic garnet powder in a tubular oven using a lockable quartz-tube inlay. Already, during the cool down ramp, the calcined LLZO powder was held under argon in order to avoid direct contact with ambient air, thereby suppressing  $\text{Li}_2\text{CO}_3$  formation on the LLZO. Subsequently, the calcined LLZO powder that is placed under argon inside the lockable quartz tube was transferred into the argon filled glovebox ( $\text{H}_2\text{O}$  and  $\text{O}_2 < 0.1$  ppm). All further processing steps were carried out in the glovebox environment to avoid contamination with moisture from the air.

**2. Procedure for  $\text{Li}^+/\text{H}^+$  Exchange by Solvent Treatment.** To induce  $\text{Li}^+/\text{H}^+$  cation exchange of the Al-stabilized cubic LLZO garnet on solvent treatment, 1 g of the pristine LLZO was weighed into glass vials ( $V_{\text{vial}} = 40$  mL) inside the glovebox. The corresponding amount of the solvents, i.e., 0.2 mol, was added to the powders before the vials were sealed. Besides high purity water (Millipore) as the treatment medium, the following solvents were used: methanol (MeOH, reagent grade, 100%, VWR Prolabo Chemicals), ethanol (EtOH, absolute, dried, max. 0.01%  $\text{H}_2\text{O}$ , >99.9%, Merck), 1-propanol (n-PrOH, puriss, >99%, Merck), 2-propanol (i-PrOH, reagent grade, 100%, VWR Prolabo Chemicals), acetonitrile (AcN, anhydrous, >99.8%, Sigma-Aldrich), and cyclohexane (c-Hex, reagent grade, 99.9%, VWR Prolabo Chemicals). The solvents were stored in the glovebox and dried using molecular sieves (3 Å). All dispersions were stirred on a vibrating plate for 2 weeks to provoke more significant changes in  $\text{Li}^+/\text{H}^+$  compositions. After 2 weeks, the solid

phase and solution were separated by filtration. No additional solvents were introduced for washing since this would have inevitably changed the LLZO/solvent ratio. This step was carried out in ambient atmosphere, but care was taken to limit the exposure time of the powder to air to a minimum. Therefore, the filtered and still solvent-wetted LLZO pastes were transferred immediately after filtration back to the glovebox for drying. In the end, the powder was dried overnight in an oven at 60 °C in a glovebox environment.

**3. Sample Characterization.** Thermogravimetric/mass spectrometry analysis (TGA-MS) of the LLZO powder was performed on a Netzsch STA 449F3 apparatus using 5 K/min heating rate in Ar atmosphere in the 35–950 °C range. FT-IR analyses were performed on a Bruker Equinox 55 spectrometer in the 3600–600  $\text{cm}^{-1}$  range, averaging 32 scans per measurement. High-resolution synchrotron powder diffraction data were collected using the beamline 11-BM at the Advanced Photon Source at Argonne National Laboratory with a calibrated wavelength of 0.4126680 Å at 295 K. Discrete detectors covering an angular range from  $-6$  to  $16^\circ 2\theta$  are scanned over a  $34^\circ 2\theta$  range, with data points collected every  $0.001^\circ 2\theta$  and scan speed of  $0.1^\circ/\text{s}$ . Rietveld refinements of the obtained diffraction patterns were performed using the General Structure Analysis System II (GSAS-II).<sup>29</sup> The space group  $Ia\bar{3}d$  and the structural data of  $\text{Li}_7\text{La}_3\text{Zr}_2\text{O}_{12}$  were used as the initial structural model.<sup>30</sup> A minor amount  $\text{Li}_2\text{ZrO}_3$  was identified in all of the samples as an additional secondary phase (<2 wt %).<sup>31</sup>

Inductive coupled plasma optical emission spectroscopy (ICP-OES, 7000DV, PerkinElmer) was employed to determine the  $\text{Li}^+$  content of the pristine and solvent treated powders. Samples for ICP-OES measurements were prepared as follows. About 0.02 g of powder (pristine or solvent treated) was dissolved in *aqua regia*. The *aqua regia* for dissolving the LLZO samples is composed of a mixture of high purity hydrochloric acid (HCl, 37%, ARISTAR for trace analysis, VWR Chemicals) and nitric acid ( $\text{HNO}_3$ , 67%, NORMATOM for trace metal analysis, VWR Chemicals). The molar ratio of HCl: $\text{HNO}_3$  is 3:1. The solution was stirred at room temperature overnight until the powder was fully dissolved. Then, the solution was diluted before use. In the course of the ICP-OES analyses the diluted sample solutions were delivered to the plasma applying 1.5 mL/min flow rate. Since detection at 610.362 nm resulted in a lower quality spectrum, detection at 670.784 nm provided high quality signal for lithium. For all samples, three parallel measurements were performed for the better statistics, and the arithmetic average of the measurement results was calculated. The calculated standard deviations of the three parallel analyses fall into the 0.003–0.010 mg/L range and correspond to 0.5–1.7%. The stability of the plasma was controlled using an internal standard by adding 1 mg/L yttrium. The signal was detected at  $\lambda = 371.029$  nm.

**4. Computational Details ab Initio Calculations.** The CRYSTAL17 code<sup>32</sup> was adopted for all the ab initio calculations in its massively parallel implementation.<sup>33</sup> All calculations were performed within the Density Functional Theory, adopting the Becke, 3 parameters, Lee–Yang–Parr (B3LYP) hybrid functional.<sup>34</sup> The tolerance for the SCF cycle convergence has been kept at the default value of  $10^{-7}$  Ha. Values of the tolerances that control the Coulomb and exchange series in periodical systems were set to  $10^{-7}$  and  $10^{-14}$  Ha, respectively.<sup>35</sup> The Hamiltonian matrix was diagonalized using 8k points (shrinking factor = 2).<sup>36</sup> Li and O were described by all-electron split valence double- $\zeta$  basis sets: 6-11G for the former<sup>37</sup> and 6-31G(d,p) for the latter.<sup>38</sup> An Ahlrichs's pVDZ basis was used for H.<sup>39</sup> Hay–Wadt small-core pseudopotentials were employed for Zr and La.<sup>40</sup> The Zr  $4s^2 4p^6 4d^2 5s^2$  and La  $5s^2 5p^6 5d^1 6s^2$  electrons were treated explicitly in order to take into account the pressure-induced relaxations of the outer core electrons.<sup>41,42</sup> Both cell parameters and internal coordinates were optimized, using the analytical gradient method. Although, due to the modeling procedure, the space group for cubic LLZO had to be set to P1, with all atoms in the crystallographic unit cell included in the irreducible unit, cubic constraints ( $a = b = c$  and  $\alpha = \beta = \gamma = 90^\circ$ ) were maintained during the optimization. Default convergence values were used for the maximum allowed gradient, the maximum atomic displacement and

their maximum allowed root-mean-square values for convergence ( $0.00045$  Ha-bohr $^{-1}$ ,  $0.00180$  Bohr,  $0.00030$  Ha-bohr $^{-1}$ , and  $0.00120$  Bohr, respectively). The choice of the computational approach, allowed by the efficient implementation of hybrid functionals and all electron basis sets in the CRYSTAL code, was guided by the requirement of high accuracy in the prediction of the cell parameters.

## RESULTS AND DISCUSSION

### I. Structural and Chemical Composition Analyses.

Since laboratory X-ray diffraction is not suitable for the accurate and thorough structural study of the partially protonated garnet phases, high-resolution synchrotron powder diffraction data were collected. Structural changes such as alteration of the lattice parameters and phase purity of the Al-substituted LLZO upon Li-ion extraction were assessed for the pristine and for each solvent treated sample. A representative synchrotron diffraction pattern of the pristine LLZO using a Rietveld refinement can be found in Figure 1.

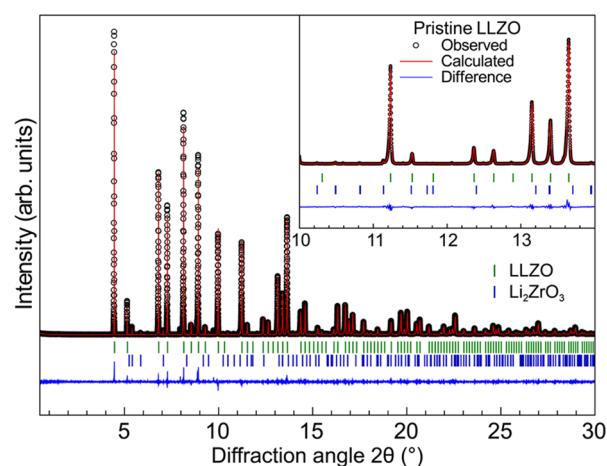


**Figure 1.** Representative Rietveld refinement for the pristine LLZO, including profile fit and profile difference using three LLZO phases and the impurity phase  $\text{Li}_2\text{ZrO}_3$ . The top ticks are for the majority LLZO (LLZO1) phase and the bottom ones are for the La-deficient minor impurity  $\text{Li}_2\text{ZrO}_3$ . The inset is showing a magnified region of the same representative fit.  $R_{\text{wp}} = 9.40\%$ , and  $\text{GoF} = 2.17$ . Obtained phase fractions are  $\text{LLZO1}:\text{LLZO2}:\text{LLZO3}:\text{Li}_2\text{ZrO}_3 = 82.7:12.6:3.0:1.7$ .

The diffraction patterns of all samples exhibit a high degree of asymmetry which leads to a “shoulder” at lower diffraction angle as demonstrated in Figure 2a. This asymmetry cannot be described sufficiently by the instrumental asymmetry, suggesting that it belongs to the targeted LLZO phase itself. The asymmetry itself cannot be properly fit with a single cubic garnet phase (i.e., LLZO1, see Figure 2a). By adding two additional cubic garnet phases (LLZO2 and LLZO3), i.e., the exact same structure with only slightly larger lattice constants, as secondary LLZO phases significantly improves the fit. This *multiphase fitting approach* necessitates manual centering of the lattice parameters and is shown in Figure 2b,c using the representative fits of the reflection from (400) Miller plane; however, the asymmetry can be found in all Bragg reflections with sufficient intensity. In Figure 2b the result of the fit with one additional LLZO phase (LLZO2) with a lattice parameter larger by  $0.02966$  Å is presented. In Figure 2c the fit with the further third LLZO phases (LLZO3) with a lattice constant larger than LLZO2 by  $0.03289$  Å is represented. We attribute

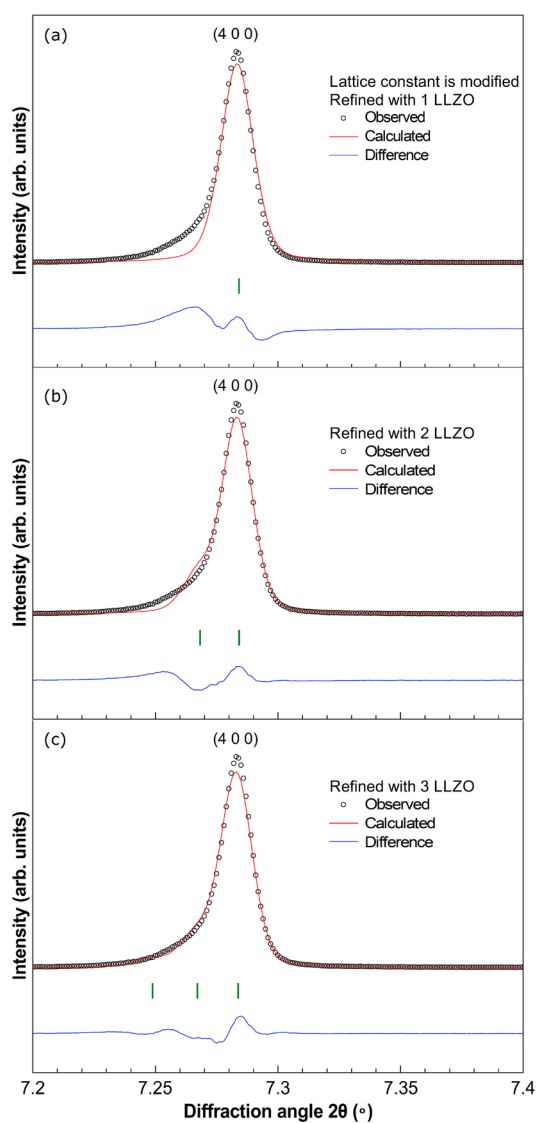


**Figure 2.** Representative synchrotron diffraction patterns and corresponding Rietveld refinement shown for the reflection of the (400) Miller plane as obtained from the pristine, nontreated (“pristine”) LLZO. (a) A lattice constant of the majority LLZO (LLZO1) is adjusted to fit the reflection. (b) Fit with an additional LLZO phase (LLZO2) with a lattice parameter larger by 0.02966 Å. (c) Fit with one more LLZO phases (LLZO3) with a lattice constant larger than LLZO2 by 0.03289 Å. The fit is significantly improved by including additional LLZO phases for a given lattice constant of LLZO1, showing a nondiscrete spread in lattice parameters due to  $\text{Li}^+/\text{H}^+$  exchange. The fit with three LLZO was then used as a reference to assess the degree of asymmetry of peaks from solvent treated samples.

this distribution of unit-cell parameters to the known instability of these lithium conducting garnets in humid (ambient) atmosphere,<sup>16,25,26,43,44</sup> as the resulting  $\text{Li}^+/\text{H}^+$  exchange is known to lead to an increase in the unit-cell parameters. In reality, while three phases are used to describe the asymmetry the resulting phases likely represent a continuous spread of nondiscrete lattices in LLZO as previously observed for the garnets.<sup>45</sup> The difference in the lattice parameters of the main phase and the secondary phases are in the range of 0.06 Å. For an overview, only the lattice parameters of the majority phase are reported in Table 1.

**Table 1.**  $\text{Li}^+/\text{H}^+$  Compositions in the Pristine and Solvent Treated LLZO Samples, Lattice Constants, and the Refined Parameters from the Rietveld Analyses Based on Synchrotron Data

| sample and treatment method | residual $\text{Li}^+/\text{H}^+$ content <sup>a</sup> | lattice parameter $a^b$ (Å) |
|-----------------------------|--|-----------------------------|
| pristine (nontreated)       | $\text{Li}_{5.90}\text{H}_{0.35}$                      | 12.9927                     |
| $\text{H}_2\text{O}$        | $\text{Li}_{4.67}\text{H}_{1.23}$                      | 12.9995                     |
| MeOH                        | $\text{Li}_{4.68}\text{H}_{1.22}$                      | 12.9965                     |
| EtOH                        | $\text{Li}_{4.70}\text{H}_{1.20}$                      | 12.9965                     |
| n-PrOH                      | $\text{Li}_{4.63}\text{H}_{1.27}$                      | 12.9965                     |
| i-PrOH                      | $\text{Li}_{5.45}\text{H}_{0.45}$                      | 12.9930                     |
| AcN                         | $\text{Li}_{5.50}\text{H}_{0.40}$                      | 12.9930                     |
| c-Hex                       | $\text{Li}_{5.40}\text{H}_{0.50}$                      | 12.9935                     |

<sup>a</sup>From the ICP-OES analyses after solvent treatment. <sup>b</sup>Based on synchrotron data.

In order to understand the occurring changes in the samples in different solvent media, the following procedure was performed: the changes in the lattice parameters and degree of peak asymmetry of differently processed samples were addressed by shifting only the lattice parameters with the fixed phase fractions (LLZO1:LLZO2:LLZO3 = 82.7:12.6:3.0), as obtained from the Rietveld refinement of the pristine, nontreated LLZO sample, while retaining the differences in the lattice parameters of main and secondary phases ( $a(\text{LLZO2}) - a(\text{LLZO1}) = 0.02966$  Å and  $a(\text{LLZO3}) - a(\text{LLZO2}) = 0.03289$  Å), and instrumental parameters obtained from pristine LLZO.

Figure 3 shows a zoom into the (400) reflections of all samples processed in the different solvents. Two main observations can be made, i.e., a remarkable shift in the maximum of the (400) reflection, as well as a growing peak asymmetry, depending on the solvent. Diffraction data in Figure 3 demonstrate that certain solvents affect the crystal structure of the LLZO more severely, for instance, protic polar solvents, such as  $\text{H}_2\text{O}$ , and primary, short-chain aliphatic alcohol homologues (i.e., MeOH, EtOH, n-PrOH). Regarding these samples, the peak shift of the (400) reflection compared to the pristine, nontreated LLZO (the center of the peak position is marked with the dashed line) and the rather high peak asymmetry is obvious. The apparent shift in the  $2\theta$ -position of the reflection can be attributed to a more severe  $\text{Li}^+/\text{H}^+$  exchange. Shifting of the peak maximum to lower diffraction angles indicates the increasing unit cell parameters, which originate from the partial substitution of Li-ions with protons in the host LLZO (cf. Table 1). Furthermore, the growing asymmetry of the (400) reflection is the result of the nondiscrete spread in lattice parameters of the LLZO caused by the more severe  $\text{Li}^+/\text{H}^+$  exchange. The nonideal peak shape, i.e., growing asymmetry can further be correlated to a degree of “cleanliness” of the LLZO after treatment in the solvents.

Protic solvents with readily available  $-\text{OH}$  functional groups are a good source for protons compared to aprotic solvents; hence, the  $\text{Li}^+/\text{H}^+$  cation exchange occurs with a larger magnitude. On the other hand, treatment with other solvents such as aprotic polar (i.e., AcN) or nonpolar (i.e., c-Hex) results in lower  $\text{Li}^+/\text{H}^+$  exchange rate and, therefore, in smaller changes of chemical composition and crystal lattice parameters. The latter is demonstrated by the less significant peak shift of the (400) reflection and the less pronounced peak asymmetry (see in Figure 3).

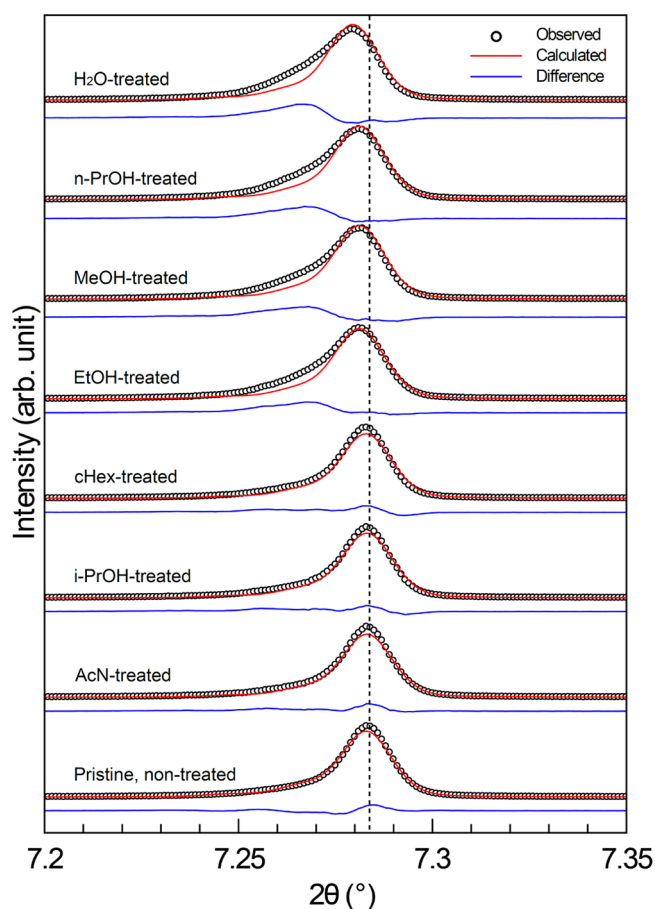


**Figure 3.** Representative patterns for the (400) reflections including profile fit and profile residuals of the corresponding refinements. The dashed-black line indicates the position of the (400) reflection from the pristine LLZO with  $a = 12.9927$  Å. The degree of peak asymmetry as well as the lattice parameter of the majority phase grows with more protic solvents.

Noteworthy is that, among the used solvents containing –OH functional groups in the present study, the less polar secondary alcohol, *i*-PrOH, shows rather weak ability for  $\text{Li}^+/\text{H}^+$  exchange. However, its regioisomer *n*-PrOH possesses strong capability to leach Li-ions from the LLZO crystals. Comparing the Li-ion leaching strength of the solvents *n*-PrOH and *i*-PrOH (with quite similar physicochemical properties), the secondary alcohol *i*-PrOH causes less pronounced changes in the chemical composition, and thereby alteration in lattice parameters of the LLZO during solvent treatment. It is assumed, that this effect could be accounted for the weaker acidic character of the secondary alcohol, *i*-PrOH. Nevertheless, due to the conformational differences between *n*-PrOH and *i*-PrOH, the lower  $\text{Li}^+/\text{H}^+$  exchange rate for *i*-PrOH could be discussed in terms of steric hindrance, as well. In summary, protic solvents with stronger acidic character (i.e.,  $\text{H}_2\text{O}$ , MeOH, EtOH, *n*-PrOH) result in more severe compositional changes, i.e.,  $\text{Li}^+/\text{H}^+$  exchange reactions, whereas aprotic and nonpolar solvents such as AcN and *c*-Hex can preserve the pristine LLZO structure.

The observed crystallographic changes in the LLZO samples on solvent treatment were correlated to their chemical compositions. We assumed that the peak shift, as it is demonstrated in Figure 3, is a direct consequence of the  $\text{Li}^+/\text{H}^+$  cation exchange in the host LLZO, and thus, it must be

reflected in the determined residual Li-ion concentrations of the samples after solvent treatments. Therefore, ICP-OES analyses have been carried out to quantitatively analyze residual Li-ion content of the solid phases after solvent treatments of the pristine LLZO.

In the present study the targeted, theoretical composition of the as-synthesized LLZO (i.e., pristine, nontreated) is  $\text{Li}_x\text{Al}_{0.25}\text{La}_3\text{Zr}_2\text{O}_{12}$ , where  $x = 6.25$ . Based on the results from the ICP-OES measurements, the Li-ion content for the pristine, nontreated LLZO along with the solvent treated powder samples were determined as presented in Figure 4. The calculated stoichiometric proportion for lithium ( $x$ ) is displayed as the blue columns. The red bars show the calculated stoichiometric amounts ( $y$ ) for protons in the  $\text{Li}_x\text{H}_y\text{Al}_{0.25}\text{La}_3\text{Zr}_2\text{O}_{12}$  compounds. The calculated amount of protons is based on the electronic charge neutrality of the material. Based on the ICP-OES data for the pristine LLZO powder, a lithium concentration corresponding to  $x = 5.9$   $\text{Li}^+$  per formula was determined. The value is slightly lower than the targeted  $x = 6.25$ . Lithium loss is expected during the high temperature calcination step of the LLZO precursors, despite using an excess amount of Li precursor in the course of the synthesis. In fact, charges must be balanced in the LLZO crystal lattice; thus, it is assumed that already in the pristine, nontreated sample a partial  $\text{H}^+$  substitution has occurred. Indeed, it has already been shown that, in the synchrotron diffraction result, a certain cation exchange must have occurred already in the pristine powder (see Figure 1). The necessity of inclusion of multiple LLZO phases for a satisfactory fit is a clear indication of the lower phase purity and mixed phase character of the sample. The partial protonation, i.e.,  $\text{Li}^+/\text{H}^+$  exchange in the pristine LLZO sample, originates supposedly from the ambient atmosphere (some steps of the sample preparation procedure has been carried out under ambient atmosphere) or from the amorphous, mixed-hydroxide precipitate mediated wet-chemical processing route of the LLZO. Therefore, the overall initial composition of pristine, nontreated powder more likely corresponds to  $\text{Li}_{5.90}\text{H}_{0.35}\text{Al}_{0.25}\text{La}_3\text{Zr}_2\text{O}_{12}$ .

In case of the solvent treated powders, the Li-ion compositions determined by ICP-OES show a good agreement with the order of crystallographic characteristics (cf. Figure 3) and phase purity. The determined lattice parameters ( $a$ ) from the Rietveld refinements (cf. Table 1) are also represented in Figure 4 (please note, dashed line is only for the purpose of better readability of the data points). Regarding the LLZO samples dispersed in *i*-PrOH, AcN, and *c*Hex, lattice parameters show quite similar values as expected from the residual lithium concentrations determined by ICP-OES, which are, in fact, close to the value of the pristine LLZO. On the other hand, MeOH, EtOH, and *n*-PrOH treated LLZO samples show larger deviations from the pristine LLZO with respect to residual lithium content. For these three samples, the lowest amounts of residual Li-ion content were determined. According to the larger shift in the position of the (400) reflection, as it is shown in Figure 3, increased lattice parameters and, thereby, significant lattice volume expansion have been ascertained.

As already seen in the diffraction data, the highest Li-ion loss in the LLZO is detected after the treatment with *n*-PrOH (22%), with only about 4.63  $\text{Li}^+$  per formula unit remaining in the sample. In general, the lithium loss is high for primary alcohols (i.e., MeOH, EtOH, *n*-PrOH) and less pronounced

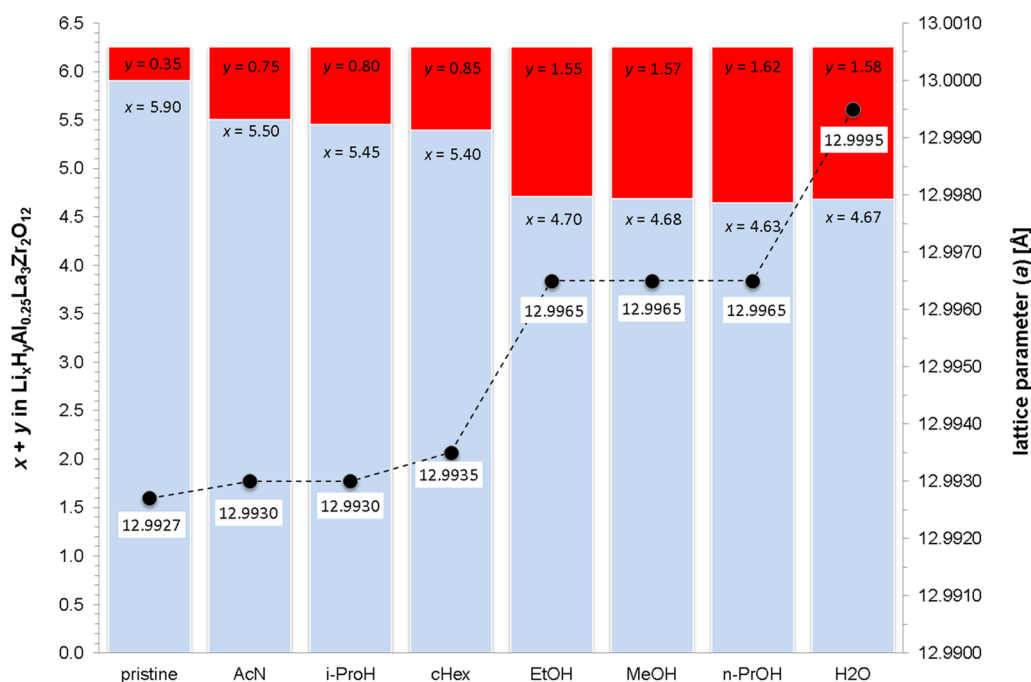
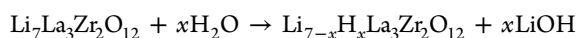


**Figure 4.** Calculated residual lithium stoichiometry of the LLZO powder samples determined by ICP-OES analyses ( $x$  values) and lattice parameter ( $a$ ) obtained from Rietveld refinement of the synchrotron diffraction data ( $y$  values are calculated based on electronic charge neutrality of the compounds).

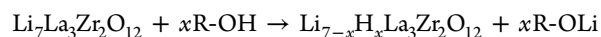
for the other organic solvents (i.e., i-PrOH, AcN, c-Hex). The Li-ion loss in all cases is assumed to be the result of a  $\text{Li}^+/\text{H}^+$  cation exchange process that has been described for LLZO before,<sup>46</sup> e.g., for Sn containing garnets.<sup>25</sup> In Sn containing garnets ( $\text{Li}_7\text{La}_3\text{Sn}_2\text{O}_{12}$ ), 68% (4.75) of the Li-ions can be exchanged for  $\text{H}^+$  ions using ethanol/benzoic acid solution. In contrast, in Ta-substituted LLZO, only four Li-ions can be removed from the crystal structure by water.<sup>47</sup> The difference between the value reported here and previous studies may be the variation in elements (Zr vs Sn), a variation in solvent/LLZO concentration, or exchange conditions (heated under reflux for 1 week in ref 25). From the results above, it is obvious that primary hydroxyl-group containing organic solvents cause significant losses in Li-ion content in the lithium-bearing garnets and by using less polar solvents the Li-ion loss is reduced drastically.

In the special case of water treatment of the LLZO, the determined lattice parameter from the Rietveld refinement of the synchrotron diffraction data suggests much higher lithium loss than was determined by ICP-OES analysis. Among the investigated samples in the present study, water agitated LLZO powder exhibits the largest lattice parameter ( $a = 12.9995 \text{ \AA}$ ) and, thereby, the highest rate of  $\text{Li}^+/\text{H}^+$  exchange. Nevertheless, residual lithium concentration after water treatment is in the same range as for the lithium content of the LLZO samples treated with primary, short-chain aliphatic alcohols. It is assumed that the reaction between LLZO and water molecules can be described with the following equation:



followed by the reaction between LiOH and dissolved  $\text{CO}_2$  in the aqueous phase to  $\text{Li}_2\text{CO}_3$ . The formed  $\text{Li}_2\text{CO}_3$  can deposit and accumulate on the surface of the LLZO particles. The formation and accumulation of  $\text{Li}_2\text{CO}_3$  on the LLZO are also evidenced by exposing the powder to ambient air. Simulta-

neous TGA-MS analyses showed that above  $300 \text{ }^\circ\text{C}$  decomposition of the superficial  $\text{Li}_2\text{CO}_3$  occurs with the concomitant release of  $\text{CO}_2$  as one of the decomposition products (see Figure S1). In the case of the water treated sample, presumably, in the beginning of the treatment procedure the formed  $\text{Li}_2\text{CO}_3$  might be dissolved in the aqueous phase. However, after the concentration of the dissolved  $\text{Li}_2\text{CO}_3$  reaches the saturation limit in the aqueous phase, the formed  $\text{Li}_2\text{CO}_3$  (i.e., due to the still ongoing  $\text{Li}^+/\text{H}^+$  exchange) deposits on the surface of the dispersed particles due to solubility issues. In fact, the presence of the formed superficial carbonate species (e.g., originating from the formed  $\text{Li}_2\text{CO}_3$ ) has been ascertained by FT-IR measurements; see Figure S2. This, in turn, results in two phenomena. First, the detection of the carbonate containing surface film on the LLZO grains is hardly possible by diffraction techniques (i.e., laboratory XRD or synchrotron diffraction), but in fact, it contaminates the sample. Second, this superficial carbonate deposition on the LLZO particles causes positive errors by the ICP-OES analyses, suggesting less Li-extraction from the LLZO phase. All lithium species found in the solid phase will be detected and analyzed by the ICP-OES measurement irrespective of their origin, i.e., originating from the solvent treated LLZO or from superficial  $\text{Li}_2\text{CO}_3$  film. However, in reality, a much higher Li-ion extraction could occur from the LLZO that the ICP-OES data suggests. This latter is evidenced by the significant enlargement of the unit cell lattice parameter for the water treated LLZO (see Figure 4). In contrast, by treatment with primary, short-chain aliphatic alcohols, such as MeOH, EtOH, and n-PrOH, the following reaction with LLZO is assumed:



where  $\text{R} = -\text{CH}_3$  (Me),  $-\text{C}_2\text{H}_5$  (Et), or  $-\text{C}_3\text{H}_7$  (Pr). The formed Li-alkoxide species will be dissolved in the correspond-

ing liquid phase and, therefore, removed from the LLZO/solvent dispersion, i.e., during the mechanical phase separation, afterward. Accumulation of the Li-alkoxide molecules by adsorption on the partially protonated LLZO is supposed to be negligible.

In summary, water treatment has probably the largest impact on the LLZO structure and results in the highest level of lithium leaching from the pristine LLZO structure. Accordingly, it is hypothesized, the Li-ion conduction of the water treated LLZO diminishes significantly, and it loses its functionality as possible solid-state electrolyte. In the case of using short-chain, primary alcohols, the extent of the Li<sup>+</sup> extraction from the LLZO was less pronounced compared to the effect of water, but still significant. A substantial change in the Li-ion conductivity of those samples has to be considered. By using aprotic polar solvents or apolar solvents the degree of Li<sup>+</sup>/H<sup>+</sup> exchange was found to be low. Therefore, in view of structural retention, those solvents are more suitable for further wet postprocessing of LLZO, suggesting a sustainable Li-ion conduction of the solid-state electrolyte material.

**II. Computational Studies.** The changes in LLZO lattice parameters due to the Li<sup>+</sup>/H<sup>+</sup> exchange as observed from the diffraction analyses were further supported by quantum mechanical simulations. The main goal was to confirm that the perceived increase of the lattice parameters and the concomitant expansion of the unit cell in cubic LLZO upon solvent treatment are indeed due to the supposed Li<sup>+</sup>/H<sup>+</sup> exchange. Furthermore, the underlying mechanisms are elucidated by atomistic insights.

At the initial step, to find the sufficient base model for the cubic LLZO is a rather difficult procedure, because in this phase the Li sublattice is always disordered. Experimentally, occupancies lower than one have been determined for cubic LLZO.<sup>48</sup> Indeed, two different types of Li symmetry sites exist in cubic LLZO: tetrahedral “Li1” (24d) and displaced octahedral “Li2” (96h) sites, accounting for a total of 120 crystallographic positions for just 56 Li-ions per unit cell.<sup>49</sup> Experimental and computational investigations have been performed in the past to define “rules” governing the occupation of the Li sites.<sup>49–53</sup> According to simulation studies in literature, however, no significant effect on the computed properties was observed by choosing different ion arrangements.<sup>52</sup> For this reason, in the present simulations, only one possible configuration has been chosen. Starting from the experimental crystal structure by Buschmann et al.<sup>48</sup> we distributed the 56 Li-ions in the cell according to the procedure suggested by Xu et al.,<sup>51</sup> 24 Li-ions were distributed over the tetrahedral “Li1” (24d) sites, and the remaining 32 ions were randomly distributed over the octahedral “Li2” (96h) sites with the constraint that Li-ion pairs cannot occupy adjacent 96h sites due to unfavorable electrostatic repulsion.

The resulting unit cell after performing a geometry optimization is reported in Figure 5 ( $x = 7.0$ ). In accordance with previous results,<sup>51</sup> the relaxation causes significant displacements of the Li-ions, so that in the end the configuration is quite different from the initial guess. Despite this, the predicted cell parameter is in extremely good agreement with the starting experimental structure ( $\Delta a = 0.0035 \text{ \AA}$ ), validating both the model and the chosen level of theory. Indeed, since very subtle volume changes are predicted as an effect of Li<sup>+</sup>/H<sup>+</sup> exchange, a high precision in the cell parameter prediction is a strong requirement for our simulations.

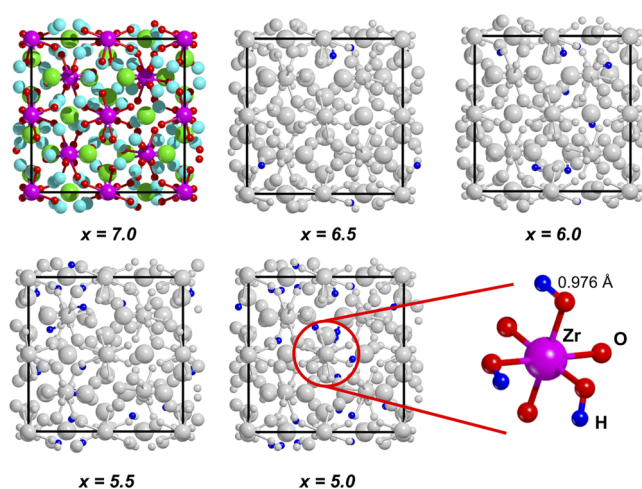


**Figure 5.** Optimized geometries of the models for the pristine ( $x = 7.0$ ) and proton substituted cubic LLZO at various degrees of substitution, identified by the value of the  $x$  subscript in the sum formula  $\text{Li}_x\text{H}_{7-x}\text{La}_3\text{Zr}_2\text{O}_{12}$ . Color code: Li, cyan; H, blue; La, green; Zr, magenta; O, red; cell borders in black. For the proton substituted structures, only the protons are highlighted, while the rest of the structure is reported in gray. Only one among the tested proton configurations, for each value of  $x$ , is reported, for simplicity. A magnification of a  $\text{ZrO}_8$  octahedron is included, to show the formation of OH groups after ion substitution.

Starting from the optimized cubic LLZO crystal structure, the proposed Li<sup>+</sup>/H<sup>+</sup> exchange mechanism has been modeled. In a random fashion, Li-ions have been replaced by H<sup>+</sup>, at various degrees of substitution, i.e., 4, 8, 12, and 16 substitutions per unit cell, corresponding to  $x = 6.5, 6, 5.5,$  and  $5$  in the sum formula of  $\text{Li}_x\text{H}_{7-x}\text{La}_3\text{Zr}_2\text{O}_{12}$ . For each value of  $x$ , at least 10 different random configurations were tested, taking then the average value of lattice parameter “ $a$ ” and using the standard deviation to estimate the error. One structure per degree of substitution is reported in Figure 5, and the variation of the cell parameter “ $a$ ” with respect to  $x$  is shown in Figure 6.

A clear linear correlation (adjusted  $R^2 = 0.991$ ) is observed between the two variables, i.e., the cell volume increases linearly with the degree of Li<sup>+</sup>/H<sup>+</sup> ion substitution. The size of the error bars shows that the chosen level of theory is capable of capturing the overall trend in the change of the lattice parameter upon Li<sup>+</sup>/H<sup>+</sup> exchange, despite only a  $0.04 \text{ \AA}$  increase in lattice parameter being observed from  $x = 7$  to  $x = 5$ . Both the trend and the absolute values of the cell parameter increases are in remarkable agreement with the experimental findings, upholding the hypothesis that LLZO experiences a process of Li<sup>+</sup>/H<sup>+</sup> exchange when treated in protic solvents. Note that the  $\text{Al}^{3+}$  substitutions in the above simulations were not included. Therefore, the values of  $x$  are not fully comparable with the experimentally obtained ones (every  $\text{Al}^{3+}$  ion replaces three Li-ions in the unit cell). A fully Li<sup>+</sup>/H<sup>+</sup> exchanged system was also modeled ( $x = 0$ ), resulting in a lattice parameter of  $13.1682 \text{ \AA}$ , suggesting that the linear trend would continue for higher degrees of substitution. However, under experimental conditions the synthesis of a pure and entirely protonated “hydrogarnet-like” phase was seemingly not possible, but its existence should not be ruled out.<sup>26</sup> Regarding the reason behind the volume increase in response to the Li<sup>+</sup>/H<sup>+</sup> exchange, a comparison between the starting substituted geometries (not shown here) and the optimized ones of Figure 5 suggests that it is dominated by ion

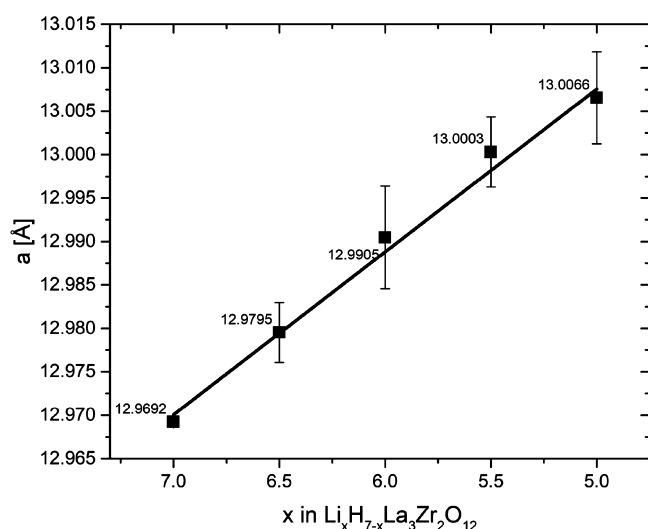


**Figure 6.** Dependence of the lattice constant “ $a$ ” in cubic LLZO on the degree of  $\text{Li}^+/\text{H}^+$  substitution, identified by the value of the  $x$  subscript in the sum formula  $\text{Li}_x\text{H}_{7-x}\text{La}_3\text{Zr}_2\text{O}_{12}$ . For each value of  $x$ , different configurations were tested, resulting in the reported average value of “ $a$ ” and in a standard deviation, visualized as an error bar. A linear fit (adjusted  $R^2 = 0.991$ ) is also included.

rearrangements. Indeed, when only the cell of an  $x = 5$  substituted model was allowed to relax, keeping the atomic positions fixed at those in pristine LLZO, a lattice parameter of 12.8863 Å was computed, smaller than the unsubstituted case. In contrast, an average lattice parameter of 13.0066 Å is obtained when all atomic positions were allowed to relax (cf. Figure 5). Particularly, the newly inserted  $\text{H}^+$  ions move toward the oxygen atoms of the  $\text{ZrO}_8$  units forming  $-\text{OH}$  groups (new  $\text{O}-\text{H}$  distance  $\approx 0.98$  Å), which can be observed in Figure 5. The formation of covalent bonds between the  $\text{H}^+$  ions and the  $\text{ZrO}_8$  units, if confirmed, could suggest a lower mobility of the protons with respect to the Li-ions they replace. In turn, this could mean that the loss in Li-ion conductivity would not be compensated by  $\text{H}^+$  conductivity, after substitution.

## CONCLUSIONS

In the present systematic study, the chemical compatibility of the Li-ion conductive garnet solid state electrolyte in different solvents is reported. By the selection of the solvents, their chemical character in terms of polarity and presence/absence of  $-\text{OH}$  bearing functional groups was decisive. The Al-substituted cubic  $\text{Li}_7\text{La}_3\text{Zr}_2\text{O}_{12}$  (LLZO) was treated with equimolar amounts of solvents with different chemistries. Refined data from the synchrotron diffraction studies pointed out that the Bragg (400) reflection is shifted to significantly lower diffraction angles upon treatment of the LLZO with polar protic solvents. Concomitantly, an increasing peak asymmetry was ascertained. The continuous spread of the nondiscrete lattices for the pristine and also solvent treated LLZO samples could be fitted by using the multiphase fitting approach. The lattice parameter ( $a$ ) for the major LLZO phase was found to increase with higher magnitude of Li-ion leaching from the pristine LLZO. This finding is in good agreement with the chemical compositions (i.e., determined residual Li-ion content) of the solvent treated LLZO samples. Ab initio computational studies supported the hypotheses, that  $\text{Li}^+/\text{H}^+$  cation exchange in the pristine LLZO results in increase of the

lattice parameter,  $a$ , and causes expansion of the unit cell volume. In fact, the chemical bond between the introduced  $\text{H}^+$  ions and  $\text{ZrO}_8$  units in the LLZO tends to have rather covalent character, which could result in lower ionic mobility. Hence, a diminished ionic conductivity of the solvent treated LLZO is predicted. We found that treatment of the LLZO with common, high purity water results in the highest deterioration of its crystal structure and also functionality in respect to Li-ion conduction. Based on our studies, we assume that aprotic polar solvents must be used by the wet postprocessing of the Li-ion conductive garnets, in order to retain its chemical structure and full functionality as a solid state electrolyte. In the case of wet-processing of polymer/ceramic hybrid solid state electrolytes, acetonitrile, for instance, would be a good choice as the dispersion medium and solvent. It has low impact on the LLZO structure, and it is a good solvent for many lithium salts and also polymers, such as PEO.

## ASSOCIATED CONTENT

### Supporting Information

The Supporting Information is available free of charge on the ACS Publications website at DOI: 10.1021/acsami.8b09789.

(Figure S1) TGA-MS analyses of the LLZO powder stored under ambient air and (Figures S2) FT-IR analyses of the pristine non-solvent-treated LLZO and the water treated sample (red solid line) (PDF)

## AUTHOR INFORMATION

### Corresponding Author

\*(R.K.) E-mail: robert.kun@uni-bremen.de.

### ORCID

Robert Kun: 0000-0002-5082-3422

Massimo Delle Piane: 0000-0001-8522-9047

Saneyuki Ohno: 0000-0001-8192-996X

Wolfgang G. Zeier: 0000-0001-7749-5089

Lucio Colombi Ciacchi: 0000-0003-1444-9733

### Notes

The authors declare no competing financial interest.

## ACKNOWLEDGMENTS

This research has been supported by the Institutional Strategy of the University of Bremen “Ambitious and Agile”, funded by the German Excellence Initiative (DFG ZUK66/1). Use of the Advanced Photon Source at Argonne National Laboratory was supported by the U.S. Department of Energy, Office of Science, Office of Basic Energy Sciences, under Contract No. DE-AC02-06CH11357. The developers of the CRYSTAL17 code, particularly the Theoretical Chemistry Group at the University of Torino, Italy, are acknowledged for providing developmental versions of the software and for technical assistance.

## REFERENCES

- (1) Janek, J.; Zeier, W. G. A Solid Future for Battery Development. *Nature Energy* **2016**, *1*, 16141.
- (2) Murugan, R.; Thangadurai, V.; Weppner, W. Schnelle Lithiumionenleitung in Granatartigem  $\text{Li}_7\text{La}_3\text{Zr}_2\text{O}_{12}$ . *Angew. Chem.* **2007**, *119*, 7925–7928.
- (3) Langer, F.; Glenneberg, J.; Bardenhagen, I.; Kun, R. Synthesis of Single Phase Cubic Al-substituted  $\text{Li}_7\text{La}_3\text{Zr}_2\text{O}_{12}$  by Solid State Lithiation of Mixed Hydroxides. *J. Alloys Compd.* **2015**, *645*, 64–69.

- (4) Rettenwander, D.; Redhammer, G.; Preishuber-Pflugl, F.; Cheng, L.; Miara, L.; Wagner, R.; Welzl, A.; Suard, E.; Doeff, M. M.; Wilkening, M.; Fleig, J.; Amthauer, G. Structural and Electrochemical Consequences of Al and Ga Cosubstitution in  $\text{Li}_7\text{La}_3\text{Zr}_2\text{O}_{12}$  Solid Electrolytes. *Chem. Mater.* **2016**, *28*, 2384–2392.
- (5) Reinacher, J.; Berendts, S.; Janek, J. Preparation and Electrical Properties of Garnet-type  $\text{Li}_6\text{BaLa}_2\text{Ta}_2\text{O}_{12}$  Lithium Solid Electrolyte Thin Films Prepared by Pulsed Laser Deposition. *Solid State Ionics* **2014**, *258*, 1–7.
- (6) Langer, F.; Bardenhagen, I.; Glenneberg, J.; Kun, R. Microstructure and Temperature Dependent Lithium Ion Transport of Ceramic–Polymer Composite Electrolyte for Solid-State Lithium Ion Batteries Based on Garnet-type  $\text{Li}_7\text{La}_3\text{Zr}_2\text{O}_{12}$ . *Solid State Ionics* **2016**, *291*, 8–13.
- (7) Tao, X.; Liu, Y.; Liu, W.; Zhou, G.; Zhao, J.; Lin, D.; Zu, C.; Sheng, O.; Zhang, W.; Lee, H. W.; Cui, Y. Solid-State Lithium–Sulfur Batteries Operated at 37 °C with Composites of Nanostructured  $\text{Li}_7\text{La}_3\text{Zr}_2\text{O}_{12}$ /Carbon Foam and Polymer. *Nano Lett.* **2017**, *17*, 2967–2972.
- (8) Zheng, J.; Tang, M.; Hu, Y. Y. Lithium Ion Pathway within  $\text{Li}_7\text{La}_3\text{Zr}_2\text{O}_{12}$ -Polyethylene Oxide Composite Electrolytes. *Angew. Chem., Int. Ed.* **2016**, *55*, 12538–12542.
- (9) Choi, J. H.; Lee, C. H.; Yu, J. H.; Doh, C. H.; Lee, S. M. Enhancement of Ionic Conductivity of Composite Membranes for All-Solid-State Lithium Rechargeable Batteries Incorporating Tetragonal  $\text{Li}_7\text{La}_3\text{Zr}_2\text{O}_{12}$  into a Polyethylene Oxide Matrix. *J. Power Sources* **2015**, *274*, 458–463.
- (10) Zhang, J.; Zhao, N.; Zhang, M.; Li, Y.; Chu, P. K.; Guo, X.; Di, Z.; Wang, X.; Li, H. Flexible and Ion-Conducting Membrane Electrolytes for Solid-State Lithium Batteries: Dispersion of Garnet Nanoparticles in Insulating Polyethylene Oxide. *Nano Energy* **2016**, *28*, 447–454.
- (11) Keller, M.; Appetecchi, G. B.; Kim, G. T.; Sharova, V.; Schneider, M.; Schuhmacher, J.; Roters, A.; Passerini, S. Electrochemical Performance of a Solvent-Free Hybrid Ceramic–Polymer Electrolyte Based on  $\text{Li}_7\text{La}_3\text{Zr}_2\text{O}_{12}$  in  $\text{P}(\text{EO})_{15}\text{LiTFSI}$ . *J. Power Sources* **2017**, *353*, 287–297.
- (12) Chen, L.; Li, Y.; Li, S. P.; Fan, L. Z.; Nan, C. W.; Goodenough, J. B. PEO/Garnet Composite Electrolytes for Solid-State Lithium Batteries: From “Ceramic-in-Polymer” to “Polymer-in-Ceramic”. *Nano Energy* **2018**, *46*, 176–184.
- (13) Fu, K. K.; Gong, Y.; Dai, J.; Gong, A.; Han, X.; Yao, Y.; Wang, C.; Wang, Y.; Chen, Y.; Yan, C.; Li, Y.; Wachsmann, E. D.; Hu, L. Flexible, Solid-State, Ion-Conducting Membrane with 3D Garnet Nanofiber Networks for Lithium Batteries. *Proc. Natl. Acad. Sci. U. S. A.* **2016**, *113*, 7094–7099.
- (14) Yang, T.; Zheng, J.; Cheng, Q.; Hu, Y. Y.; Chan, C. K. Composite Polymer Electrolytes with  $\text{Li}_7\text{La}_3\text{Zr}_2\text{O}_{12}$  Garnet-Type Nanowires as Ceramic Fillers: Mechanism of Conductivity Enhancement and Role of Doping and Morphology. *ACS Appl. Mater. Interfaces* **2017**, *9*, 21773–21780.
- (15) Chan, C. K.; Yang, T.; Weller, J. M. Nanostructured Garnet-type  $\text{Li}_7\text{La}_3\text{Zr}_2\text{O}_{12}$ : Synthesis, Properties, and Opportunities as Electrolytes for Li-ion Batteries. *Electrochim. Acta* **2017**, *253*, 268–280.
- (16) Larraz, G.; Orera, A.; Sanjuán, M. L. Cubic Phases of Garnet-Type  $\text{Li}_7\text{La}_3\text{Zr}_2\text{O}_{12}$ : the Role of Hydration. *J. Mater. Chem. A* **2013**, *1*, 11419–11428.
- (17) Wang, Y.; Lai, W. Phase Transition in Lithium Garnet Oxide Ionic Conductors  $\text{Li}_7\text{La}_3\text{Zr}_2\text{O}_{12}$ : The Role of Ta Substitution and  $\text{H}_2\text{O}/\text{CO}_2$  Exposure. *J. Power Sources* **2015**, *275*, 612–620.
- (18) Jin, Y.; McGinn, P. J.  $\text{Li}_7\text{La}_3\text{Zr}_2\text{O}_{12}$  Electrolyte Stability in Air and Fabrication of a  $\text{Li}/\text{Li}_7\text{La}_3\text{Zr}_2\text{O}_{12}/\text{Cu}_{0.1}\text{V}_2\text{O}_5$  Solid-State Battery. *J. Power Sources* **2013**, *239*, 326–331.
- (19) Cheng, L.; Crumlin, E. J.; Chen, W.; Qiao, R.; Hou, H.; Lux, S. F.; Zorba, V.; Russo, R.; Kostecki, R.; Liu, Z.; Persson, K.; Yang, W.; Cabana, J.; Richardson, T. J.; Chen, G.; Doeff, M. The Origin of High Electrolyte–Electrode Interfacial Resistances in Lithium Cells Containing Garnet Type Solid Electrolytes. *Phys. Chem. Chem. Phys.* **2014**, *16*, 18294–18300.
- (20) Cheng, L.; Wu, C. H.; Jarry, A.; Chen, W.; Ye, Y.; Zhu, J.; Kostecki, R.; Persson, K.; Guo, J.; Salmeron, M.; Chen, G.; Doeff, M. Interrelationships among Grain Size, Surface Composition, Air Stability, and Interfacial Resistance of Al-Substituted  $\text{Li}_7\text{La}_3\text{Zr}_2\text{O}_{12}$  Solid Electrolytes. *ACS Appl. Mater. Interfaces* **2015**, *7*, 17649–17655.
- (21) Uhlenbruck, S.; Dellen, C.; Möller, S.; Lobe, S.; Tsai, C. L.; Finsterbusch, M.; Bram, M.; Guillon, O. Reactions of Garnet-Based Solid-State Lithium Electrolytes with Water - A Depth-Resolved Study. *Solid State Ionics* **2018**, *320*, 259–265.
- (22) Brugge, R. H.; Hekselman, A. K. O.; Cavallaro, A.; Pesci, F. M.; Chater, R. J.; Kilner, J. A.; Aguadero, A. Garnet Electrolytes for Solid State Batteries: Visualization of Moisture-Induced Chemical Degradation and Revealing Its Impact on the Li-Ion Dynamics. *Chem. Mater.* **2018**, *30*, 3704–3713.
- (23) Yi, E.; Wang, W.; Kieffer, J.; Laine, R. M. Flame Made Nanoparticles Permit Processing of Dense, Flexible,  $\text{Li}^+$  Conducting Ceramic Electrolyte Thin Films of Cubic- $\text{Li}_7\text{La}_3\text{Zr}_2\text{O}_{12}$  (c-LLZO). *J. Mater. Chem. A* **2016**, *4*, 12947–12954.
- (24) Yi, E.; Wang, W.; Kieffer, J.; Laine, R. M. Key Parameters Governing the Densification of Cubic- $\text{Li}_7\text{La}_3\text{Zr}_2\text{O}_{12}$   $\text{Li}^+$  Conductors. *J. Power Sources* **2017**, *352*, 156–164.
- (25) Galven, C.; Dittmer, J.; Suard, E.; Le Berre, F.; Crosnier-Lopez, M.-P. Instability of Lithium Garnets against Moisture. Structural Characterization and Dynamics of  $\text{Li}_{7-x}\text{H}_x\text{La}_3\text{Sn}_2\text{O}_{12}$  and  $\text{Li}_{5-x}\text{H}_x\text{La}_3\text{Nb}_2\text{O}_{12}$ . *Chem. Mater.* **2012**, *24*, 3335–3345.
- (26) Galven, C.; Fourquet, J.-L.; Crosnier-Lopez, M.-P.; Le Berre, F. Instability of the Lithium Garnet  $\text{Li}_7\text{La}_3\text{Sn}_2\text{O}_{12}$ :  $\text{Li}^+/\text{H}^+$  Exchange and Structural Study. *Chem. Mater.* **2011**, *23*, 1892–1900.
- (27) Orera, A.; Larraz, G.; Rodriguez-Velamazan, J. A.; Campo, J.; Sanjuan, M. L. Influence of  $\text{Li}^+$  and  $\text{H}^+$  Distribution on the Crystal Structure of  $\text{Li}_{7-x}\text{H}_x\text{La}_3\text{Zr}_2\text{O}_{12}$  ( $0 \leq x \leq 5$ ) Garnets. *Inorg. Chem.* **2016**, *55*, 1324–1332.
- (28) Hofstetter, K.; Samson, A. J.; Narayanan, S.; Thangadurai, V. Present Understanding of the Stability of Li-stuffed Garnets with Moisture, Carbon Dioxide, and Metallic Lithium. *J. Power Sources* **2018**, *390*, 297–312.
- (29) Toby, B. H.; Von Dreele, B. R. GSAS-II: the Genesis of a Modern Open-Source All Purpose Crystallography Software Package. *J. Appl. Crystallogr.* **2013**, *46*, 544–549.
- (30) Xie, H.; Alonso, J. A.; Li, Y.; Fernández-Díaz, M. T.; Goodenough, J. B. Lithium Distribution in Aluminum-Free Cubic  $\text{Li}_7\text{La}_3\text{Zr}_2\text{O}_{12}$ . *Chem. Mater.* **2011**, *23*, 3587–3589.
- (31) Heiba, Z. K.; El-Sayed, K. Structural and Anisotropic Thermal Expansion Correlation of  $\text{Li}_2\text{ZrO}_3$  at Different Temperatures. *J. Appl. Crystallogr.* **2002**, *35*, 634–636.
- (32) Dovesi, R.; Orlando, R.; Erba, A.; Zicovich-Wilson, C. M.; Civalieri, B.; Casassa, S.; Maschio, L.; Ferrabone, M.; De La Pierre, M.; D’Arco, P.; Noel, Y.; Causa, M.; Rerat, M.; Kirtman, B. CRYSTAL14: A Program for the Ab Initio Investigation of Crystalline Solids. *Int. J. Quantum Chem.* **2014**, *114*, 1287–1317.
- (33) Orlando, R.; Delle Piane, M.; Bush, I. J.; Ugliengo, P.; Ferrabone, M.; Dovesi, R. A New Massively Parallel Version of CRYSTAL for Large Systems on High Performance Computing Architectures. *J. Comput. Chem.* **2012**, *33*, 2276–2284.
- (34) Becke, A. D. Density-Functional Thermochemistry. III. The Role of Exact Exchange. *J. Chem. Phys.* **1993**, *98*, 5648–5652.
- (35) Dovesi, R.; Saunders, V. R.; Roetti, C.; Orlando, R.; Zicovich-Wilson, C. M.; Pascale, F.; Civalieri, B.; Doll, K.; Harrison, N. M.; Bush, I. J.; D’Arco, P.; Llunel, M.; Causa, M.; Noel, Y. CRYSTAL14, *User’s Manual*; Università di Torino: Torino, Italy, 2014.
- (36) Monkhorst, H. J.; Pack, J. D. Special Points for Brillouin-Zone Integrations. *Phys. Rev. B* **1976**, *13*, 5188–5192.
- (37) Ojamäe, L.; Hermansson, K.; Pisani, C.; Causà, M.; Roetti, C. Structural, Vibrational and Electronic Properties of a Crystalline Hydrate from Ab Initio Periodic Hartree-Fock Calculations. *Acta Crystallogr., Sect. B: Struct. Sci.* **1994**, *50*, 268–279.

- (38) Francl, M. M.; Pietro, W. J.; Hehre, W. J.; Binkley, J. S.; Gordon, M. S.; De Frees, D. J.; Pople, J. A. Self-Consistent Molecular Orbital Methods. XXIII. A Polarization-Type Basis Set for Second-Row Elements. *J. Chem. Phys.* **1982**, *77*, 3654–3665.
- (39) Schäfer, A.; Horn, H.; Ahlrichs, R. Fully Optimized Contracted Gaussian Basis Sets for Atoms Li to Kr. *J. Chem. Phys.* **1992**, *97*, 2571–2577.
- (40) Hay, P. J.; Wadt, W. R. Ab Initio Effective Core Potentials for Molecular Calculations. Potentials for the Transition Metal Atoms Sc to Hg. *J. Chem. Phys.* **1985**, *82*, 270–283.
- (41) Sophia, G.; Baranek, P.; Sarrazin, C.; Rerat, M.; Dovesi, R. First-Principles Study of the Mechanisms of the Pressure-Induced Dielectric Anomalies in Ferroelectric Perovskites. *Phase Transitions* **2013**, *86*, 1069–1084.
- (42) Evarestov, R. A.; Kotomin, E. A.; Matrikov, Y. A.; Gryaznov, D.; Heifets, E.; Maier, J. Comparative Density-Functional LCAO and Plane-Wave Calculations of LaMnO<sub>3</sub> surfaces. *Phys. Rev. B: Condens. Matter Mater. Phys.* **2005**, *72*, 214411.
- (43) Wang, W. G.; Wang, X. P.; Gao, Y. X.; Yang, J. F.; Fang, Q. F. Investigation on the Stability of Li<sub>5</sub>La<sub>3</sub>Ta<sub>2</sub>O<sub>12</sub> Lithium Ionic Conductors in Humid Environment. *Front. Mater. Sci. China* **2010**, *4*, 189–192.
- (44) Truong, L.; Thangadurai, V. Soft-Chemistry of Garnet-Type Li<sub>5+x</sub>Ba<sub>x</sub>La<sub>3-x</sub>Nb<sub>2</sub>O<sub>12</sub> (x = 0, 0.5, 1): Reversible H<sup>+</sup> ↔ Li<sup>+</sup> Ion-Exchange Reaction and Their X-ray, <sup>7</sup>Li MAS NMR, IR, and AC Impedance Spectroscopy Characterization. *Chem. Mater.* **2011**, *23*, 3970–3977.
- (45) Zeier, W. G.; Zhou, S.; Lopez-Bermudez, B.; Page, K.; Melot, B. C. Dependence of the Li-Ion Conductivity and Activation Energies on the Crystal Structure and Ionic Radii in Li<sub>6</sub>MLa<sub>2</sub>Ta<sub>2</sub>O<sub>12</sub>. *ACS Appl. Mater. Interfaces* **2014**, *6*, 10900–10907.
- (46) Nemori, H.; Matsuda, Y.; Mitsuoka, S.; Matsui, M.; Yamamoto, O.; Takeda, Y.; Imanishi, N. Stability of Garnet-Type Solid Electrolyte Li<sub>x</sub>La<sub>3</sub>A<sub>2-y</sub>B<sub>y</sub>O<sub>12</sub> (A = Nb or Ta, B = Sc or Zr). *Solid State Ionics* **2015**, *282*, 7–12.
- (47) Yow, Z. F.; Oh, Y. L.; Gu, W.; Rao, R. P.; Adams, S. Effect of Li<sup>+</sup>/H<sup>+</sup> Exchange in Water Treated Ta-doped Li<sub>7</sub>La<sub>3</sub>Zr<sub>2</sub>O<sub>12</sub>. *Solid State Ionics* **2016**, *292*, 122–129.
- (48) Buschmann, H.; Dölle, J.; Berendts, S.; Kuhn, A.; Bottke, P.; Wilkening, M.; Heitjans, P.; Senyshyn, A.; Ehrenberg, H.; Lotnyk, A.; Duppel, V.; Kienle, L.; Janek, J. Structure and Dynamics of the Fast Lithium Ion Conductor "Li<sub>7</sub>La<sub>3</sub>Zr<sub>2</sub>O<sub>12</sub>". *Phys. Chem. Chem. Phys.* **2011**, *13*, 19378–19392.
- (49) Bernstein, N.; Johannes, M. D.; Hoang, K. Origin of the Structural Phase Transition in Li<sub>7</sub>La<sub>3</sub>Zr<sub>2</sub>O<sub>12</sub>. *Phys. Rev. Lett.* **2012**, *109*, 205702.
- (50) Kang, S. G.; Sholl, D. S. First-Principles Study of Chemical Stability of the Lithium Oxide Garnets Li<sub>7</sub>La<sub>3</sub>M<sub>2</sub>O<sub>12</sub> (M = Zr, Sn, or Hf). *J. Phys. Chem. C* **2014**, *118*, 17402–17406.
- (51) Xu, M.; Park, M. S.; Lee, J. M.; Kim, T. Y.; Park, Y. S.; Ma, E. Mechanisms of Li<sup>+</sup> Transport in Garnet-Type Cubic Li<sub>3+x</sub>La<sub>3</sub>M<sub>2</sub>O<sub>12</sub> (M = Te, Nb, Zr). *Phys. Rev. B: Condens. Matter Mater. Phys.* **2012**, *85*, 052301.
- (52) Rettenwander, D.; Blaha, P.; Laskowski, R.; Schwarz, K.; Bottke, P.; Wilkening, M.; Geiger, C. A.; Amthauer, G. DFT Study of the Role of Al<sup>3+</sup> in the Fast Ion-Conductor Li<sub>7-3x</sub>Al<sup>3+</sup><sub>x</sub>La<sub>3</sub>Zr<sub>2</sub>O<sub>12</sub> Garnet. *Chem. Mater.* **2014**, *26*, 2617–2623.
- (53) Meier, K.; Laino, T.; Curioni, A. Solid-State Electrolytes: Revealing the Mechanisms of Li-Ion Conduction in Tetragonal and Cubic LLZO by First-Principles Calculations. *J. Phys. Chem. C* **2014**, *118*, 6668–6679.